Int. J. Solids Structures Vol. 23, No. 8, pp. 1145–1161, 1987
Printed in Great Britain.

0020-7683/87 $3.00+ .00

AN APPROXIMATE METHOD FOR PREDICTION OF TRANSVERSE SHEAR STRESSES IN A LAMINATED SHELL

REAZ A. CHAUDHURI
Department of Civil Engineering, University of Utah, Salt Lake City, UT 84112, U.S.A.

and

PAUL SEIDE
Department of Civil Engineering, University of Southern California, Los Angeles, CA 90089-114, U.S.A.

(*Received* 6 *September* 1985; *in revised form* 5 *December* 1986)

Abstract—A method has been presented wherein the surface-parallel stresses in a laminated shell are first computed using standard finite element formulation and then approximate transverse shear stress variation through the shell thickness is obtained utilizing the first two (stress) equations of equilibrium and divergence theorem. Numerical results have been presented for both homogeneous isotropic and laminated anisotropic cylindrical shells using the Cartesian-like Riemann coordinate approximation and compared to the corresponding analytical solutions.

NOMENCLATURE

$A_j^{(i)}$	total surface area of the jth triangular layer element belonging to the ith layer
$[C^{(i)}]$	elastic (material) stiffness matrix of the ith anisotropic layer
C_{ij}	elements of $[C]$
$\{d_j^{(i)}\}$	nodal displacement vector for the jth layer element belonging to the ith layer
E	Young's modulus of an isotropic material
E_{ij}	elastic modulus of an anisotropic material (stretching)
G_{ij}	shear moduli of an anisotropic material
$\mathbf{g}_m$	tangent (to the α-, β-, ζ-curves) vectors
g_{mn}	metric tensor
g^{mn}	associated metric tensor
$\bar{g}_{11}, \bar{g}_{22}$	first fundamental quantities of the shell reference surface for lines of curvature co-ordinates
$\mathbf{i}_r$	orthonormal basis vectors for fixed Cartesian coordinates
L	length of a cylindrical shell
$\bar{n}_r$	rth physical component of unit normal vector
N	total number of layers
N'	number of subdivisions
p	uniform internal pressure
R	inner radius of a cylindrical shell
$1/R_\alpha, 1/R_\beta$	normal curvatures of the reference surface in the directions of the lines of curvature
$1/R_\Gamma, 1/R_n, 1/R_{n\Gamma}$	normal curvatures and twist of the reference surface parallel and normal to the direction of the boundary curve
$S_j^{(i)}(\zeta)$	area of the jth layer element belonging to the ith layer at a distance ζ from the bottom of the layer
t	total thickness of a laminated shell
t_i	thickness of the ith layer
$V_j^{(i)}$	volume of the jth triangular layer element belonging to the ith layer
x, y	Cartesian-like local Riemann coordinates in the directions of the lines of curvature α and β, respectively
z, ζ	transverse coordinate direction
x, θ, z	circular cylindrical shell coordinates
α, β	lines of curvature coordinates measured on the shell reference surface
$\Gamma_j^{(i)}(\zeta)$	perimeter of the jth layer element belonging to the ith layer at a distance ζ from the bottom surface of the layer
Γ_{lp}^m	Euclidean–Christoffel symbol
$\gamma_{\alpha\zeta}^{(i)}, \gamma_{\beta\zeta}^{(i)}$	transverse shearing strains in the ith layer
$\varepsilon_\alpha^{(i)}(\zeta), \gamma_{\alpha\beta}^{(i)}(\zeta), \varepsilon_\beta^{(i)}(\zeta)$	strains of line elements, originally in the α- and β-directions, located at a distance ζ from the bottom of the ith layer
$\eta_l(\zeta)$	covariant components of unit vector normal to the element boundary
$\eta_{3l}(\zeta)$	covariant components of unit vector normal to the ζ-surface
θ_i	fiber orientation in the ith layer measured with respect to the α-direction

ν	Poisson's ratio for an isotropic material
ν_{12}, ν_{21}	major and minor Poisson's ratio, respectively, in the surface of the fibers
$\sigma_\alpha^{(\rho)}(\zeta), \sigma_\beta^{(\rho)}(\zeta), \tau_{\alpha\beta}^{(\rho)}(\zeta)$	surface-parallel components of stresses
τ^{lm}	contravariant components of stress tensor
$\tau_{\alpha\zeta}^{(\rho)}(\zeta), \tau_{\beta\zeta}^{(\rho)}(\zeta)$	physical components of transverse shear stresses
ϕ	angle between the boundary curve Γ and the α-direction.

INTRODUCTION

The study of variation of transverse (interlaminar) shear stresses through the thickness of a laminated shell has assumed increasing importance, because such a shell is more likely to fail due to delamination caused by the scissoring effect of these stresses, especially in the vicinity of free edges. Analytical solutions[1–9] are mostly restricted to simple shell geometry (e.g. cylindrical and spherical shells). A laminated general shell solution[10] that has recently become available is restricted to shallow shell geometry, cross-ply lamination and simply supported boundary conditions. A numerical procedure, such as the finite element method (FEM) seems to be the only practical alternative because of the ease with which problems of general shell geometry, irregular shapes, non-uniform thickness, anisotropy, arbitrary lamination, complex boundary conditions and general loadings can be handled by this method. A review of the literature, however, suggests that short of conducting a highly refined three-dimensional analysis, few FEM based methods are available which yield accurate transverse shear stress variation through the thickness of a general laminated shell. An assumed linear displacement triangular element due to Seide and Chang[11] can only compute constant transverse shear stresses through the thickness of each layer. The quadrilateral element due to Mau *et al.*[12] based on an assumed stress hybrid approach has the capability of predicting the transverse shear stress variation through the thickness of a thick multi-layer plate, by considering stresses as unknown nodal parameters and imposing constraints on the compatibility of these stresses at each interface and vanishing of the transverse shear stresses on the top and bottom surfaces of the plate. However, this method appears to be limited in its applicability as the formulation of the stiffness matrix involves too many matrix inversions at the element level and extension by Spilker *et al.*[13] to the triangular element shape has produced a very stiff element. More importantly, the (normal) traction-free edge formulation has not been satisfied[13], which leads to inaccuracy in the prediction of through-thickness transverse shear stress variations near the edge[14]. Furthermore, a review of the literature suggests that neither this method nor a displacement-based method has been applied in the prediction of transverse shear stresses in a laminated shell.

Recently, Seide and Chaudhuri[15] have developed an efficient triangular shell element (plate element being a special case) based on the assumptions of transverse inextensibility and LCST (layerwise constant shear-angle theory, Fig. 1) and assumed a quadratic (in the curvilinear coordinate plane) displacement potential energy approach. Chaudhuri[14] has also discussed the use of this element in obtaining accurate transverse shear stress variation through the thickness of a thick laminated plate. The method described in Ref. [14] involves computation of in-plane stresses in a plate by using the FEM first and then the equilibrium

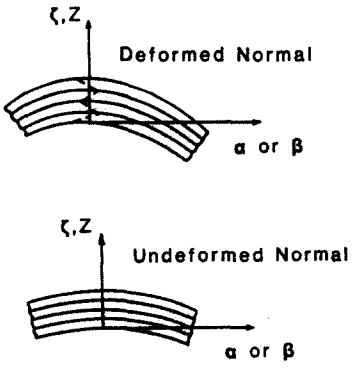

Fig. 1. Possible severe cross-sectional warping in a thick multi-layer shell.

equations for the purpose of computing transverse shear stresses. The concept of use of equilibrium equations to compute transverse shear stresses is due to Pryor and Barker[16], who utilized it for a quadrilateral symmetrically laminated plate element based on CST (constant shear-angle theory). Extension of the concept and the procedure, outlined in Ref. [14], to laminated shells is a challenge yet to be addressed. The difficulty pertaining to the behavior of solids in the Riemannian space is primarily mathematical in nature and appropriate approximations based on physical judgement must be employed to obtain reasonably accurate solutions, because deriving exact solutions is next to impossible. That is why, the authors believe, the literature is so sparse on the subject. The present paper represents the first attempt at the application of the above concept to a laminated general shell.

BACKGROUND INFORMATION

Each triangular element belonging to the ith layer is bounded by the ith and $i+1$th interfaces (Fig. 2). The present element chosen is a quadratic triangle of C^0-type in the α–β plane. Each interface triangle is characterized by six nodes, each of which is associated with three nodal displacement parameters. By virtue of the assumption of transverse inextensibility the transverse displacement w does not vary through the thickness. The number of degrees of freedom per node is then $2N+3$ for an N-layer composite shell element. The choice of quadratic shape functions (in the α–β plane) makes it possible to predict accurate transverse shear stress variation through shell thickness, achieve faster convergence of displacements and stresses and obtain solutions to more complex problems. The formulation of element matrices is not restricted to any particular shell geometry. The element can be mapped onto any curved surface, depending on the choice of metrics $\bar{g}_{11}(\alpha, \beta)$ and $\bar{g}_{22}(\alpha, \beta)$.

Details concerning formulation of the element stiffness matrix, consistent load vector, effect of numerical integration on the convergence of displacements and stresses, solution to global equations and element stresses, etc. have been presented in Refs [15, 17]. Once the displacements are determined, the element stresses can be obtained using the relation[15, 17]

$$\{\sigma^{(i)}(\zeta)\} = [C^{(i)}]\{\varepsilon^{(i)}(\zeta)\} \tag{1a}$$

where

$$\{\sigma^{(i)}(\zeta)\}^{\mathrm{T}} = \{\sigma_\alpha^{(i)}(\zeta), \sigma_\beta^{(i)}(\zeta), \tau_{\alpha\beta}^{(i)}(\zeta), \bar{\tau}_{\alpha\zeta}^{(i)}(\zeta), \bar{\tau}_{\beta\zeta}^{(i)}(\zeta)\} \tag{1b}$$

$$\{\varepsilon^{(i)}(\zeta)\}^{\mathrm{T}} = \{\varepsilon_\alpha^{(i)}(\zeta), \varepsilon_\beta^{(i)}(\zeta), \gamma_{\alpha\beta}^{(i)}(\zeta), \bar{\gamma}_{\alpha\zeta}^{(i)}(\zeta), \bar{\gamma}_{\beta\zeta}^{(i)}(\zeta)\} \tag{1c}$$

$$\{e^{(i)}(\zeta)\} = [A^{(i)}(\zeta)]\{\bar{\varepsilon}^{(i)}\}. \tag{1d}$$

$[C^{(i)}]$, $[A^{(i)}(\zeta)]$ and $\{\varepsilon^{(i)}\}$ are as given by eqns (A1), (A2) and (A4), respectively.

It is noteworthy that while accurate surface-parallel components of stresses can be computed at special points on the interface triangle, the transverse shear stress components, obtained from eqn (1), $\tau_{\alpha\zeta}^{(i)}(\zeta)$ and $\tau_{\beta\zeta}^{(i)}(\zeta)$, do not represent the true transverse shear stresses. They are essentially the physical components corrresponding to average (through thickness) covariant components of the true transverse shear stresses (the same is true for $\bar{\gamma}_{\alpha\zeta}^{(i)}(\zeta)$ and $\bar{\gamma}_{\beta\zeta}^{(i)}(\zeta)$). A method of determination of the shear stress variation through the thickness of a

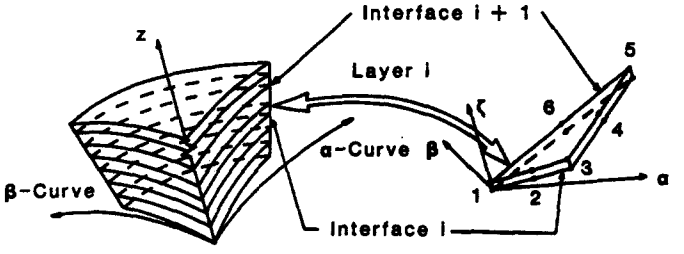

Fig. 2. Mapping of triangular element on a curved surface onto curvilinear coordinate plane.

laminated shell, using the surface-parallel components of stresses computed by the assumed displacement potential energy approach and the first two equations of equilibrium, will be presented in the following section.

METHOD OF ANALYSIS

Arbitrarily laminated general shell

Equations of equilibrium for a general shell neglecting body forces are given by[18]

$$\tau^{lm}/l = 0 \quad \text{for} \quad m,\ l = 1(\text{or } \alpha),\ 2(\text{or } \beta),\ 3(\text{or } z) \tag{2}$$

where covariant derivatives of contravariant components of stresses τ^{ml}, are defined as[19]

$$\tau^{lm}/l = \tau^{lm}_{,l} + \Gamma^{m}_{lp}\tau^{lp} + \Gamma^{p}_{lp}\tau^{lm} \tag{3}$$

while the Euclidean–Christoffel symbol Γ^{m}_{lp} is defined as[18–20]

$$\Gamma^{m}_{lp} = \tfrac{1}{2}g^{mn}(g_{np,l} + g_{ln,p} + g_{lp,n}) = \Gamma^{m}_{pl} \tag{4}$$

with[17]

$$g_{11}(z) = \frac{1}{g^{11}(z)} = \bar{g}_{11}\left(1 + \frac{z}{R_\alpha}\right)^2 \tag{5a}$$

$$g_{22}(z) = \frac{1}{g^{22}(z)} = \bar{g}_{22}\left(1 + \frac{z}{R_\beta}\right)^2 \tag{5b}$$

$$g_{33}(z) = \frac{1}{\sqrt{(g^{33}(z))}} = 1 \tag{5c}$$

$$g_{mn}(z) = g^{mn}(z) = 0 \quad \text{for} \quad m \neq n. \tag{5d}$$

Relations (5) hold on account of the selection of the orthogonal curvilinear coordinate system α, β, z where α and β denote the directions of the lines of curvature of the shell reference (bottom) surface, while z denotes the direction of the normal to the reference surface. It is noteworthy that α, β and z represent the local (or element) coordinates for the N-layer composite element. For a layer element, ζ denotes the direction of the normal and is given by

$$z = \bar{d}_i + \zeta \tag{6a}$$

where

$$\bar{d}_i = \sum_{m=1}^{i-1} t_m; \qquad \bar{d}_1 = 0. \tag{6b}$$

Equation (3) contains derivatives of surface-parallel components of stresses with respect to α and β which involves additional computations. These are avoided by integration of eqn (2) over the volume of the triangular layer element and then application of the divergence (Green–Gauss) theorem, which leads to[19]

$$\iiint_{V_j^{(i)}} \tau^{lm}/l\,\mathbf{g}_m \, \mathrm{d}V_j^{(i)} = \iint_{A_j^{(i)}} \tau^{lm}\eta_l\mathbf{g}_m \, \mathrm{d}A_j^{(i)} = 0 \tag{7}$$

where[20]

$$\mathbf{g}_m = \frac{\partial x^r}{\partial \theta^m}\mathbf{i}_r \quad \text{for} \quad m, l = 1(\text{or } \alpha),\ 2(\text{or } \beta),\ 3(\text{or } \zeta) \quad \text{and also} \quad r = 1, 2, 3. \tag{8}$$

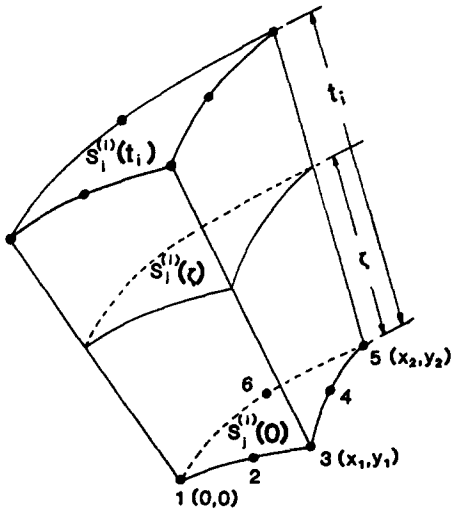

Fig. 3. The jth triangular layer element belonging to the ith layer.

Here $\theta^1 = \alpha$, $\theta^2 = \beta$, $\theta^3 = \zeta$ and x^r, $r = 1,2,3$, is a fixed Cartesian system located at the local (element) origin such that x^1 and x^2 are tangential to the α- and β-curves, respectively, at the element origin. In eqns (2)–(4) and (7), repeated indices imply summation.

We are essentially interested in the first two equations of equilibrium, since these will yield $\tau_{\alpha\zeta}^{(i)}(\zeta)$ and $\tau_{\beta\zeta}^{(i)}(\zeta)$. They correspond to $r = 1,2$ in eqns (7). For a sufficiently small element, which is reasonable to expect in most cases in practice at the time of convergence

$$\mathbf{g}_r \sim \sqrt{(g_{rr}(\zeta))}\mathbf{i}_r \quad \text{(no sum on } r\text{)} \tag{9}$$

and these two equations are written as

$$\iint_{A_j^{(i)}(\zeta)} \tau^{I1}\eta_I \sqrt{(g_{11}(\zeta))}\, \mathrm{d}A^{(i)}(\zeta) = 0 \tag{10a}$$

$$\iint_{A_j^{(i)}(\zeta)} \tau^{I2}\eta_I \sqrt{(g_{22}(\zeta))}\, \mathrm{d}A^{(i)}(\zeta) = 0. \tag{10b}$$

Referring to Fig. 3 and noting that

$$A_j^{(i)}(\zeta) \equiv S_j^{(i)}(0) + S_j^{(i)}(\zeta) + \int_\zeta \Gamma_j^{(i)}(\zeta)\, \mathrm{d}\zeta \tag{11}$$

the integrated form of the first equation of equilibrium, given by eqn (10a), can be written as

$$\begin{aligned}
&-\iint_{S_j^{(i)}(\zeta)} \tau^{31}(\zeta)\sqrt{(g_{11}(\zeta))}\eta_{\zeta 3}(\zeta)\, \mathrm{d}S^{(i)}(\zeta) + \iint_{S_j^{(i)}(0)} \tau^{31}(0)\sqrt{(g_{11}(0))}\eta_{\zeta 3}(0)\, \mathrm{d}S^{(i)}(0) \\
&= \iint_{\zeta\Gamma_j^{(i)}(\zeta)} [\tau^{11}(\zeta)\sqrt{(g_{11}(\zeta))}\eta_1(\zeta) + \tau^{21}(\zeta)\sqrt{(g_{11}(\zeta))}\eta_2(\zeta) + \tau^{31}(\zeta)\sqrt{(g_{11}(\zeta))}\eta_3(\zeta)]\, \mathrm{d}\Gamma(\zeta)\, \mathrm{d}\zeta \\
&\quad + \iint_{S_j^{(i)}(\zeta)} [\tau^{11}(\zeta)\sqrt{(g_{11}(\zeta))}\eta_{\zeta 1}(\zeta) + \tau^{21}(\zeta)\sqrt{(g_{11}(\zeta))}\eta_{\zeta 2}(\zeta)]\, \mathrm{d}S^{(i)}(\zeta) \\
&\quad - \iint_{S_j^{(i)}(0)} [\tau^{11}(0)\sqrt{(g_{11}(0))}\eta_{\zeta 1}(0) + \tau^{21}(0)\sqrt{(g_{11}(0))}\eta_{\zeta 2}(0)]\, \mathrm{d}S^{(i)}(0).
\end{aligned} \tag{12}$$

Since the normal to any surface, parallel to the reference surface of the shell, coincides with the ζ-coordinate direction

$$\eta_{\zeta 1}(\zeta) = \eta_{\zeta 2}(\zeta) = 0 \quad \text{and} \quad \eta_{\zeta 3}(\zeta) = 1 \quad \text{for} \quad 0 \leqslant \zeta \leqslant t_i, \quad i = 1, \ldots, N. \tag{13}$$

In addition, since the normal to the vertical surfaces of the triangular layer element is perpendicular to the ζ-direction

$$\eta_3(\zeta) = 0. \tag{14a}$$

The relations between the non-vanishing covariant and the physical components of the normal vector are given by[17, 18]

$$\eta_1(\zeta) = \bar{n}_1 \sqrt{\bar{g}_{11}} \left(1 + \frac{\bar{d}_i + \zeta}{R_\alpha}\right) \tag{14b}$$

$$\eta_2(\zeta) = \bar{n}_2 \sqrt{\bar{g}_{22}} \left(1 + \frac{\bar{d}_i + \zeta}{R_\beta}\right). \tag{14c}$$

The relations between the contravariant and physical components of stresses are given by[17, 18]

$$\tau^{11}(\zeta) = \frac{\sigma_\alpha(\zeta)}{\bar{g}_{11}\left(1 + \frac{\bar{d}_i + \zeta}{R_\alpha}\right)^2} \tag{15a}$$

$$\tau^{22}(\zeta) = \frac{\sigma_\beta(\zeta)}{\bar{g}_{22}\left(1 + \frac{\bar{d}_i + \zeta}{R_\beta}\right)^2} \tag{15b}$$

$$\tau^{12}(\zeta) = \frac{\tau_{\alpha\beta}(\zeta)}{\sqrt{(\bar{g}_{11}\bar{g}_{22})}\left(1 + \frac{\bar{d}_i + \zeta}{R_\alpha}\right)\left(1 + \frac{\bar{d}_i + \zeta}{R_\beta}\right)} \tag{15c}$$

$$\tau^{13}(\zeta) = \frac{\tau_{\alpha\zeta}(\zeta)}{\sqrt{\bar{g}_{11}}\left(1 + \frac{\bar{d}_i + \zeta}{R_\alpha}\right)} \tag{15d}$$

$$\tau^{23}(\zeta) = \frac{\tau_{\beta\zeta}(\zeta)}{\sqrt{\bar{g}_{22}}\left(1 + \frac{\bar{d}_i + \zeta}{R_\beta}\right)}. \tag{15e}$$

Noting that[17]

$$\mathrm{d}S^{(i)}(\zeta) = \left(1 + \frac{\bar{d}_i + \zeta}{R_\alpha}\right)\left(1 + \frac{\bar{d}_i + \zeta}{R_\beta}\right) \mathrm{d}\bar{S} \tag{16a}$$

with

$$d\bar{S} = \sqrt{(\bar{g}_{11}\bar{g}_{22})}\, d\alpha\, d\beta \tag{16b}$$

$$d\Gamma^{(i)}(\zeta) = \left[\left(1 + \frac{\bar{d}_i + \zeta}{R_\Gamma}\right)^2 + \left(\frac{\bar{d}_i + \zeta}{R_{n\Gamma}}\right)^2\right]^{1/2} d\bar{\Gamma} \tag{17}$$

while $\bar{S}_j$ and $\bar{\Gamma}_j$ are the area and perimeter, respectively, of the jth triangular element over the reference (bottom) surface of the laminated shell and $1/R_\Gamma$ and $1/R_{n\Gamma}$ are given by[15]

$$\frac{1}{R_\Gamma} = \frac{\sin^2\bar{\phi}}{R_\alpha} + \frac{\cos^2\bar{\phi}}{R_\beta} \tag{18a}$$

$$\frac{1}{R_{n\Gamma}} = -\left(\frac{1}{R_\alpha} - \frac{1}{R_\beta}\right)\sin\bar{\phi}\cos\bar{\phi}. \tag{18b}$$

Equation (12) with the help of eqns (13)–(17) can be written as

$$\int\int_{\bar{S}_j} \tau_{\alpha\zeta}^{(i)}(\zeta)\left(1 + \frac{\bar{d}_i + \zeta}{R_\alpha}\right)\left(1 + \frac{\bar{d}_i + \zeta}{R_\beta}\right) d\bar{S} = \int\int_{\bar{S}_j} \tau_{\alpha\zeta}^{(i)}(0)\left(1 + \frac{\bar{d}_i}{R_\alpha}\right)\left(1 + \frac{\bar{d}_i}{R_\beta}\right) d\bar{S}$$
$$- \int\int_{\bar{\Gamma}_j\zeta} [\sigma_\alpha^{(i)}(\zeta)\bar{n}_1 + \tau_{\alpha\beta}^{(i)}(\zeta)\bar{n}_2]\left[\left(1 + \frac{\bar{d}_i + \zeta}{R_\Gamma}\right)^2 + \left(\frac{\bar{d}_i + \zeta}{R_{n\Gamma}}\right)^2\right]^{1/2} d\zeta\, d\bar{\Gamma} \tag{19}$$

where

$$\tau_{\alpha\zeta}^{(i)}(t_i) = \tau_{\alpha\zeta}^{(i+1)}(0) \quad \text{for} \quad i = 1, \ldots, N-1 \tag{20a}$$

and

$$\tau_{\alpha\zeta}^{(1)}(0) = \tau_{\alpha\zeta}^{(N)}(t_i) = 0. \tag{20b}$$

$\tau_{\alpha\zeta}^{(1)}(0) = 0$ is used here, since integration through thickness starts from the reference surface. The remaining condition, $\tau_{\alpha\zeta}^{(N)}(t_i) = 0$, will be automatically satisfied if the surface-parallel components of stresses computed by FEM are exact.

Substituting eqns (1) and (A1)–(A3) into eqn (19) and integrating with respect to ζ will yield

$$\int\int_{\bar{S}_j} \tau_{\alpha\zeta}^{(i)}(\zeta)\left(1 + \frac{\bar{d}_i + \zeta}{R_\alpha}\right)\left(1 + \frac{\bar{d}_i + \zeta}{R_\beta}\right) d\bar{S} = \int\int_{\bar{S}_j} \tau_{\alpha\zeta}^{(i)}(0)\left(1 + \frac{\bar{d}_i}{R_\alpha}\right)\left(1 + \frac{\bar{d}_i}{R_\beta}\right) d\bar{S}$$
$$- \int_{\bar{\Gamma}_j} [\{(c_{11}^{(i)}\bar{n}_1 + c_{13}^{(i)}\bar{n}_2)\varepsilon_\alpha^{(i)}(0) + (c_{13}^{(i)}\bar{n}_1 + c_{33}^{(i)}\bar{n}_2)\gamma_\alpha^{(i)}(0)\}\{f_1^{(i)}(\zeta) - f_1^{(i)}(0)\}$$
$$+ \{(c_{12}^{(i)}\bar{n}_1 + c_{23}^{(i)}\bar{n}_2)\varepsilon_\beta^{(i)}(0) + (c_{13}^{(i)}\bar{n}_1 + c_{33}^{(i)}\bar{n}_2)\gamma_\beta^{(i)}(0)\}\{f_2^{(i)}(\zeta) - f_2^{(i)}(0)\}$$
$$+ \{(c_{11}^{(i)}\bar{n}_1 + c_{13}^{(i)}\bar{n}_2)\varepsilon_\alpha^{(i)}(t_i) + (c_{13}^{(i)}\bar{n}_1 + c_{33}^{(i)}\bar{n}_2)\gamma_\alpha^{(i)}(t_i)\}\{f_3^{(i)}(\zeta) - f_3^{(i)}(0)\}$$
$$+ \{(c_{12}^{(i)}\bar{n}_1 + c_{23}^{(i)}\bar{n}_2)\varepsilon_\beta^{(i)}(t_i) + (c_{13}^{(i)}\bar{n}_1 + c_{33}^{(i)}\bar{n}_2)\gamma_\beta^{(i)}(t_i)\}\{f_4^{(i)}(\zeta) - f_4^{(i)}(0)\}]\, d\bar{\Gamma} \tag{21}$$

where $\bar{n}_1$ and $\bar{n}_2$ at a point on each side of the triangle over the reference surface can be

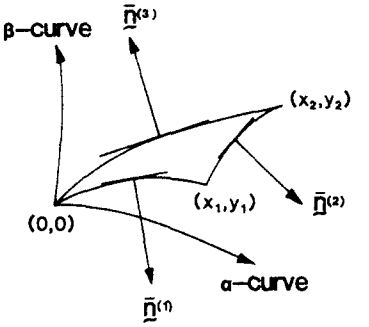

Fig. 4. A typical curved element interface.

obtained in a manner discussed in the Appendix (refer to Fig. 4). The functions $f_1^{(i)}(\zeta)$, etc. are given by eqns (A6)–(A8).

If a particular side of the triangular element is parallel to a coordinate direction α (or β), then

$$R_\Gamma = R_\alpha \text{ (or } R_\beta) \quad \text{and} \quad R_{n\Gamma} = \infty.$$

The functions $f_1^{(i)}(\zeta)$, etc. are then greatly simplified and can easily be obtained.

An equation similar to eqn (19), involving $\tau_{\beta\zeta}^{(i)}(\zeta)$, can be obtained starting from the second equation of equilibrium as given by eqn (10b).

For a flat plate, $R_\alpha = R_\beta = \infty$ and $\sqrt{\bar{g}_{11}} = \sqrt{\bar{g}_{22}} = 1$ when rectangular Cartesian coordinates are used, i.e. $\alpha = x$, $\beta = y$. It has been shown in Refs [14, 21] that for such a case, $\tau_{\alpha\zeta}^{(i)}(\zeta)$, averaged over the area of the element $\bar{S}_j$, represents the exact transverse shear stress at the centroid of the interface triangle. For a general shell, this is no longer deemed possible, because of the complexities introduced by $\bar{g}_{11}$, $\bar{g}_{22}$, R_α and R_β which are, in general, complicated functions of α and β. However, a reasonably good estimate of $\tau_{\alpha\zeta}^{(i)}(\zeta)$ (and $\tau_{\beta\zeta}^{(i)}(\zeta)$) may be obtained by evaluating the surface integral

$$\iint_{\bar{S}_j} \tau_{\alpha\zeta}^{(i)}(\zeta)\left(1+\frac{\bar{d}_i+\zeta}{R_\alpha}\right)\left(1+\frac{\bar{d}_i+\zeta}{R_\beta}\right) d\bar{S} \sim \left[\tau_{\alpha\zeta}^{(i)}(\zeta)\left(1+\frac{\bar{d}_i+\zeta}{R_\alpha}\right)\left(1+\frac{\bar{d}_i+\zeta}{R_\beta}\right)\right]\bar{S}_j. \quad (22)$$

$\tau_{\alpha\zeta}^{(i)}(\zeta)$ thus computed will represent the average transverse shear stress over the area (on the reference surface of the curved element). This will be reasonably accurate, because the area of an element becomes smaller and smaller as convergence of displacements and stresses is approached. For the numerical evaluation of the line integral, depending on the shell geometry, a sufficient number of integration points may be selected on each of the three sides of the curved element on the reference surface. This is illustrated in Ref. [14] for a flat plate. Computer implementation of the method for general shells is currently underway at the University of Utah, the outcome of which will be published in a future paper. This paper will address the approximate solution to the problem.

Shallow shell approximation

For such shells

$$\frac{\bar{d}_i+\zeta}{R_\alpha}, \frac{\bar{d}_i+\zeta}{R_\beta} \ll 1.$$

Then eqn (19) on integration with respect to ζ reduces to

$$\iint_{S_j} \tau_{\alpha\zeta}^{(i)}(\zeta)\,\mathrm{d}\bar{S} = \iint_{S_j} \tau_{\alpha\zeta}^{(i)}(0)\,\mathrm{d}\bar{S} - \iint\left[\left\{\sigma_\alpha^{(i)}(0)\left(\zeta - \frac{\zeta^2}{2t_i}\right) + \sigma_\alpha^{(i)}(t_i)\frac{\zeta^2}{2t_i}\right\}\bar{n}_1 + \left\{\tau_{\alpha\beta}^{(i)}(0)\left(\zeta - \frac{\zeta^2}{2t_i}\right) + \tau_{\alpha\beta}^{(i)}(t_i)\frac{\zeta^2}{2t_i}\right\}\bar{n}_2\right]\mathrm{d}\bar{\Gamma}. \quad (23)$$

A similar expression can be obtained for $\tau_{\beta\zeta}^{(i)}(\zeta)$. In the above equations $\sigma_\alpha^{(i)}$, etc. are obtained using eqn (1).

It is noteworthy that the above approximation renders the variation of transverse shear stresses through the thickness of each layer parabolic, which is true for a flat plate[14].

Cartesian-like local Riemann coordinates (CLRC) approximation

Every Riemann space admits Riemann coordinates for any given origin, where all the Christoffel symbols vanish[20]. The Riemann coordinates with origin, in the present context, may be defined as

$$x = x^1 = \int_0^\alpha \sqrt{\bar{g}_{11}}\,\mathrm{d}\alpha \quad \text{and} \quad y = x^2 = \int_0^\beta \sqrt{\bar{g}_{22}}\,\mathrm{d}\beta \quad (24)$$

where x and y measure geodesic (shortest) distances between any point (α, β) or (x, y) within the element and the local (element) origin along the α and β lines of curvature. These Riemann coordinates may be thought to behave like rectangular Cartesian coordinates in the vicinity of the local origin, because every Riemann space is also locally Euclidean (i.e. admits rectangular Cartesian coordinates), which implies that every sufficiently small (infinitesimally small in the limit) portion of the Riemann space is Euclidean. The above two concepts, Riemann coordinates with origin and Riemann space being locally Euclidean, may be fused into one powerful approximation in the context of FEM, because (i) each finite element is associated with local coordinates the origin of which may be located anywhere within the element and (ii) element size becomes smaller and smaller as convergence of displacements and stresses is approached. It is noteworthy that a locally Euclidean approximation alone will imply that a curved shell element is being replaced by a flat (plate) element (i.e. the effect of curvature is completely neglected), which introduces the domain approximation. The present approximation, in contrast, does not introduce any domain approximation and retains some curvature effect, while simplifying the equilibrium equations considerably.

The equations of equilibrium, under the above approximation, become the same as those for flat plates (with Cartesian coordinates) with x and y defined by eqns (24), which, following the logic in Ref. [14], may be written as

$$\begin{aligned}\tau_{\alpha\zeta}^{(i)}(\zeta) = \tau_{\alpha\zeta}^{(i)}(0) - \frac{1}{\bar{S}^j}\Bigg[&\left(\zeta - \frac{\zeta^2}{2t_i}\right)\{\sigma_\alpha^{(i)}|_{\substack{\text{node}\\2}} y_1 - \tau_{\alpha\beta}^{(i)}|_{\substack{\text{node}\\2}} x_1 \\ &+ \sigma_\alpha^{(i)}|_{\substack{\text{node}\\4}}(y_2 - y_1) - \tau_{\alpha\beta}^{(i)}|_{\substack{\text{node}\\4}}(x_2 - x_1) - \sigma_\alpha^{(i)}|_{\substack{\text{node}\\6}} y_2 + \tau_{\alpha\beta}^{(i)}|_{\substack{\text{node}\\6}} x_2\} \\ &+ \frac{\zeta^2}{2t_i}\{\sigma_\alpha^{(i+1)}|_{\substack{\text{node}\\2}} y_1 - \tau_{\alpha\beta}^{(i+1)}|_{\substack{\text{node}\\2}} x_1 + \sigma_\alpha^{(i+1)}|_{\substack{\text{node}\\4}}(y_2 - y_1) \\ &- \tau_{\alpha\beta}^{(i+1)}|_{\substack{\text{node}\\4}}(x_2 - x_1) - \sigma_\alpha^{(i)}|_{\substack{\text{node}\\6}} y_2 + \tau_{\alpha\beta}^{(i+1)}|_{\substack{\text{node}\\6}} x_2\}\Bigg]. \end{aligned} \quad (25)$$

$\tau_{\beta\zeta}^{(i)}(\zeta)$ can be obtained in a similar manner. It has also been shown in Ref. [14] that the centroid of a triangular element interface is the point of exceptional accuracy for transverse shear stresses.

NUMERICAL RESULTS AND DISCUSSIONS

Numerical results for transverse shear stresses, using the composite-shell triangular element of Refs [15, 17] encoded in the FORTRAN program SANWAT (shell analysis with accurate theory) will be presented here. The equilibrium method presented herein will be applied to sample problems and results will be compared to those obtained analytically.

Example 1. A simply supported isotropic circular cylindrical shell under uniform internal pressure

A shell problem for which a closed-form solution is available is that of axisymmetric bending of an isotropic simply supported circular cylindrical shell under uniform internal pressure (Fig. 5). The shell is free to move longitudinally at the edges. A one-dimensional element which fulfills the axisymmetric condition of independence of stresses and displacements of position around the circumference of the cylinder is obtained by combining two right-angled triangular elements as shown and imposing the condition of equal displacements in the radial and also longitudinal direction at the points having the same θ-coordinates while displacements at all nodes in the circumferential direction vanish. The central symmetry of the problem again allows the modeling to be limited to half the length of the cylindrical shell. The cylindrical shell analyzed is 20 in. long with an inner-surface radius of 10 in. and a thickness of 0.2 in. E and ν of the shell material are 30×10^6 psi and 0.3, respectively. The internal pressure is 100 psi.

Since cylindrical shells under such loading are characterized by a boundary layer effect, convergence has been studied by using coarser mesh sizes in the central portion of the cylinder and a gradually finer mesh near the edge (Fig. 6). Table 1 shows the convergence of $\tau_{xz}(z)$ at $x = L/2$, computed using the present finite element theory, with the CLRC approximation. It is interesting to observe that although integrated (through thickness) the equilibrium equation is not, in general, satisfied, by the stresses computed by the finite element theory because of the presence of mid-surface stretching, resulting in non-vanishing transverse shear stresses at one of the two exposed surfaces, those values are negligible with finer mesh sizes. In other words, in the present problem a tangential force equilibrium is almost satisfied. The slight difference (<4%) between analytical and finite element results is probably due to the facts that (i) (τ_{xz}) at $x = L/2$ computed by the finite element method is yet to converge and (ii) the present finite element analysis computes transverse shear stresses only at the centroid of the element adjacent to the edge. The analytical results based on the classical theory are obtained using eqn (2.11.1a) of Ref. [22], which, on substitution of the stresses and integration, finally becomes

$$\tau_{xz}(x,z) = \frac{E}{(1+z/R)(1-\nu^2)R}\left[-\nu\left\{2(z+t/2)+\frac{1}{2R}(z^2-t^2/4)\right\}w_{,x} + \left\{\frac{R}{2}(z^2-t^2/4)+\tfrac{1}{3}(z^3-t^3/8)\right\}w_{,xxx}\right]. \quad (26)$$

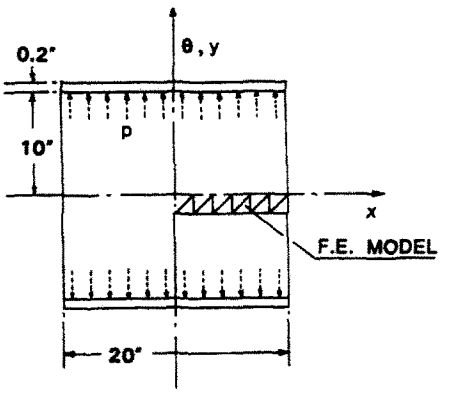

Fig. 5. A circular cylindrical shell under internal pressure.

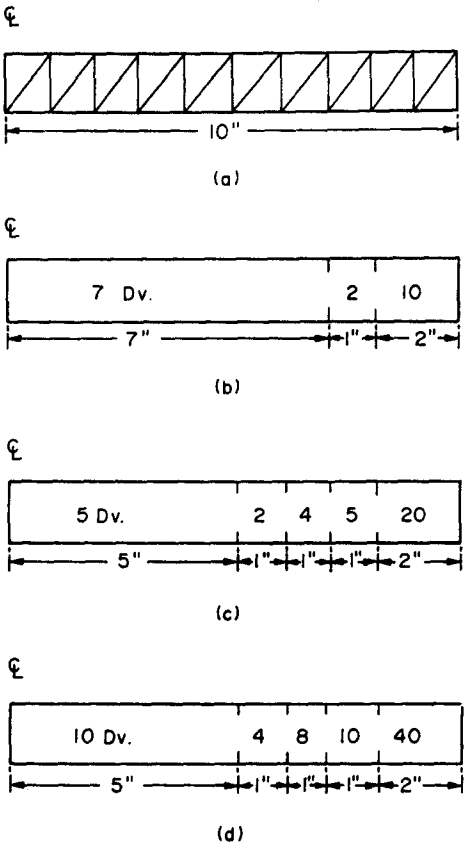

Fig. 6. Finite element models for the circular cylindrical shell under internal pressure.

Table 1. Convergence of $\tau_{xz}(z)$ at the edge of the isotropic simply supported cylindrical shell under internal pressure

R (in.)	L/Rt	$\tau_{xz}(t/2)$ at edge
10	14.14	5583.30
50	7.32	5717.96
100	4.47	5692.12
200	3.16	5716.40

"Exact" values of $\tau_{xz}(L/2, t/2)$ are obtained with and without an assumption which neglects the curvature effect and interestingly enough, this assumption yields a result, which is in close agreement with that obtained without making this assumption.

The next result is concerned with effect of $L/\sqrt{(Rt)}$ on the non-dimensionalized maximum transverse shear stress

$$(\hat{\tau}_{xz})_{\max} = \frac{(\tau_{xz})_{\max} L}{p\sqrt{(Rt)}}. \tag{27}$$

In the present investigation, the radius of the circular cylindrical shell is varied keeping the length and thickness unaltered. Table 2 shows that $\tau_{xz}(L/2, t/2)$ is, for a short cylindrical shell, almost constant for all values of $L/\sqrt{(Rt)}$. This is an extremely useful result, because transverse shear stresses in such shells need to be computed for one set of geometric parameters only.

Table 2. Effect of $L/\sqrt{(Rt)}$ on $\hat{\tau}_{xz}(t/2)$ the edge of the isotropic simply supported cylindrical shell under internal pressure

No. of divisions	$\tau_{xz}(0)$ (psi)	$\tau_{xz}(t/2)$ (psi)	$\hat{\tau}_{xz}(t)$ (psi)
10	0	−59.22	24.49
19	0	−334.98	−2.70
36	0	−376.17	−4.42
72	0	−394.86	−5.00
Classical theory (neglecting curvature effect)	0	−412.13	0
Classical theory (with curvature effect)	0	−415.20	0

Example 2. A clamped asymmetrically laminated circular cylindrical shell under uniform internal pressure

A final problem which illustrates the effect of lamination in a thin shell is that of a two-layer internally pressurized circular cylindrical shell which is supported at both edges in such a way that radial deflection and longitudinal rotation are restrained but axial stress and surface-parallel shearing stress vanish. The length of the shell and the inner radius are 20 and 10 in., respectively. The fiber reinforced layers are identical except that the inner layer has a fiber orientation in the longitudinal direction while the fiber orientation in the outer layer varies. The thickness of each layer is 0.1 in. E_{11} and E_{22} of the layer material are 40×10^6 and 10^6 psi, respectively. In-plane shear modulus, G_{12}, and transverse shear modulus, G_{13}, are assumed equal to 0.5×10^6 psi while the remaining transverse shear modulus, G_{23}, is assumed to be equal to 0.2×10^6 psi. Major Poisson's ratio, ν_{12}, defined to be ratio of strains, perpendicular and parallel to the fiber direction, caused by the stress in the direction of the fibers, is taken equal to 0.25. The displacements and stresses are independent of the circumferential coordinate, θ, but there is an additional rigid body rotation of the shell cross-sections. A closed-form solution for the problem with transverse shear deformations neglected is given in Refs [5, 23].

The finite element model chosen is similar to that of Fig. 6(d). Figures 7 and 8 show variation of $(\tau_{xz})_{\text{interface}}$ and $(\tau_{\theta z})_{\text{interface}}$ at the edge, $x = L/2$, with the fiber orientation of the outer layer, $\bar{\theta}_2$. Present FEM results are compared to the CLT solutions[23]. The difference between the two sets of results may be attributed to the approximation in obtaining the present solution and neglect of shear deformation effect in the CLT. It will be possible to offer a better explanation regarding the role of shear deformation in causing the above-mentioned difference, when FEM results using more accurate derivation for the transverse shear stresses become available in the near future.

Figures 9 and 10 show variation of τ_{xz} and $\tau_{\theta z}$, at the edge $x = L/2$, with respect to x for $\bar{\theta}_2 = 45°$. As expected, τ_{xz} and $\tau_{\theta z}$ in the boundary region of the cylindrical shell,

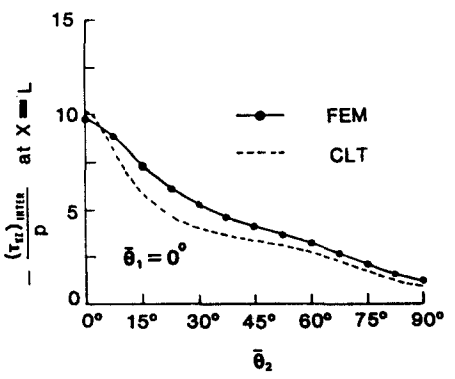

Fig. 7. Variation of $(\tau_{xz})_{\text{interface}}$ at the edge with fiber orientation of the outer layer.

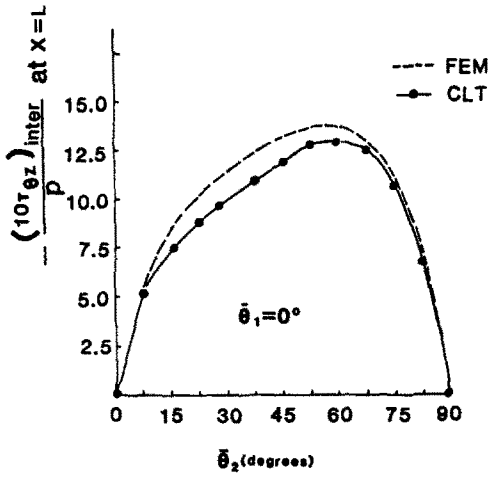

Fig. 8. Variation of $(\tau_{\theta z})_{\text{interface}}$ at the edge with fiber orientation of the outer layer.

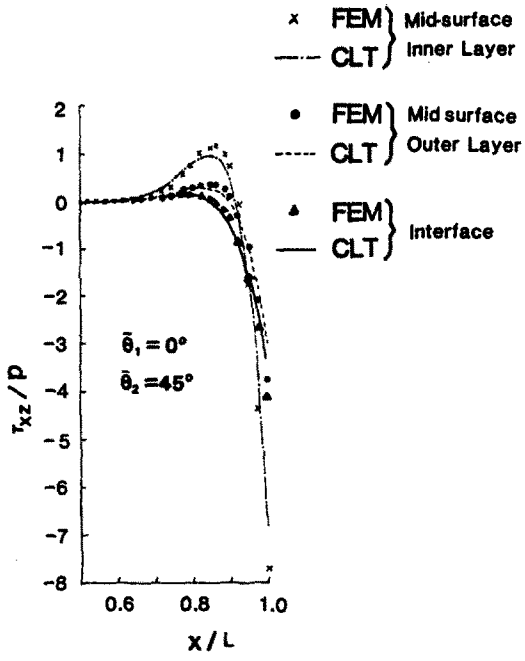

Fig. 9. Longitudinal variation of $(\tau_{xz})_{\text{interface}}$ for the two-layer cylindrical shell.

computed by the present method are in disagreement with the corresponding CLT results. This is most likely due to the shear deformation effect, which is neglected in the CLT.

Figures 11 show variation of τ_{xz} through the thickness of a two-layer cylindrical shell for $\bar{\theta}_2 = 0$, 15, 45, and 90°, with $\bar{\theta}_1 = 0°$. τ_{xz}, computed by the present method, does not completely vanish at the outer surface, as required; however, the error is negligible, which implies that the through-thickness integrated form of the equilibrium equation is nearly satisfied. It is interesting to observe the change in the shape of the curve (z vs τ_{xz}) as $\bar{\theta}_2$ varies from 0 to 90°. For the unidirectional shell ($\bar{\theta}_2 = 0$), this variation is parabolic as expected, because the shell is homogeneous. The curve has two lobes for $\bar{\theta}_2 = 15$ and 45° (looks like a split dumbell with the top half becoming thinner as $\bar{\theta}_2$ increases). For $\bar{\theta}_2 = 90°$, this curve looks like the longitudinal section of a sitar (an Indian musical instrument).

CONCLUSIONS

An approximate equilibrium method for the prediction of the transverse shear stress variation through thickness of a laminated thick shell is presented. Although the method is demonstrated for an assumed quadratic displacement triangular element based on LCST

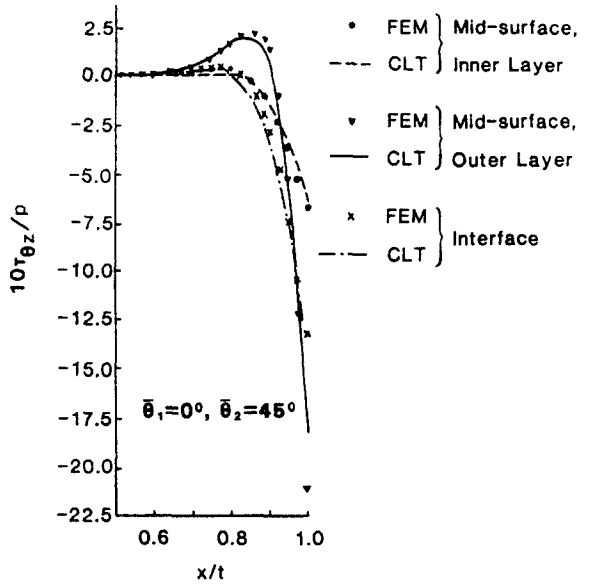

Fig. 10. Longitudinal variation of $(\tau_{\theta z})_{\text{interface}}$ for the two-layer cylindrical shell.

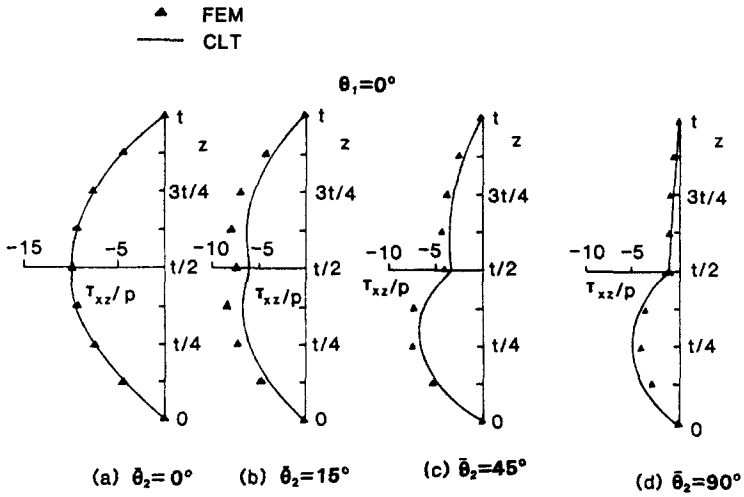

Fig. 11. Variation of $(\tau_{xz})_{\text{interface}}$ at the edge through thickness of the two-layer cylindrical shell.

and transverse inextensibility, the scope of the method is not limited to either this kind of shell theory or this particular element. In fact, the principle behind the method presented herein is applicable to any laminated shell element, once the surface-parallel components of stresses have been computed at each interface by FEM irrespective of the kind of laminated shell theory (i.e. LCST, CST or CLT) used or element shape employed in computing these stresses.

Results presented herein are based on the CLRC approximation, which gives a reasonably good estimate of the transverse shear stresses. More accurate expressions for $\tau_{\alpha\zeta}^{(i)}(\zeta)$ and $\tau_{\beta\zeta}^{(i)}(\zeta)$ for specific shell geometries are available in Ref. [17], the computer implementation of which is currently underway. These will be published in a future paper.

It may be noted that the success of this method depends on either pointwise convergence of derivatives of displacements, which will ensure satisfaction of equilibrium equations at every point or tangential force equilibrium (i.e. through-thickness integrated form of equilibrium equations) at a point on the reference surface. However, in FEM, derivatives of displacements converge only in the mean-square sense and the tangential force equilibrium at a point, as a result, may not be satisfied. Nevertheless, as has been observed in the example problems considered, the tangential force equilibrium may often be approximately satisfied. The utility of the method is that it is relatively straightforward given the complexity

of the problem under investigation. Moreover, detection of error is immediate if and when such an error arises; because, in that event, the computed transverse shear stresses will not simultaneously vanish at both the exposed surfaces. At stake here is a broader issue—the accuracy of the stresses (more precisely, the stress gradients), computed by an assumed displacement potential energy based FEM. In other words, is the local law of conservation of momentum satisfied, for a laminated anisotropic shell, with the same accuracy as the law of conservation of energy (a global law), when solutions are obtained by such a method? The present method would fail when the former law fails to be satisfied within an acceptable range of accuracy. An alternative approximate method[21], developed recently for arbitrarily laminated plates may be extended to shells and employed in such cases.

REFERENCES

1. S. A. Ambartsumyan, *Theory of Anisotropic Shells*. Moscow (1961); English translation, NASA TTF 118 (1964).
2. S. A. Ambartsumyan, Calculation of laminated anisotropic shells. *Izv. Akad. Nauk Armenskoi SSR, Ser. Fiz. Mat. Tech. Nauk* **6**, 15 (1953).
3. S. B. Dong, K. S. Pister and R. L. Taylor, On theory of laminated anisotropic shells and plates. *J. Aero. Sci.* **29**, 969 (1962).
4. S. T. Gulati and F. Essenberg, Effects of anisotropy in axisymmetric cylindrical shells. *J. Appl. Mech.* **34**, 65 (1967).
5. K. Balaraman, R. A. Chaudhuri and V. X. Kunukkasseril, Bending of asymmetrically laminated anisotropic shells subjected to internal pressure, presented at the First Conf. Reinf. Plastics and their Aero. Applic., VSSC, ISRO, Trivandrum, India (Aug. 1972).
6. R. A. Chaudhuri, Structural behavior of FRP rectangular plates and cylindrical shells. M.S. Thesis, Dept. Aero. Engng I.I.T, Madras, India (1974).
7. S. B. Dong and F. K. W. Tso, On a laminated orthotropic shell theory including transverse shear deformation. *J. Appl. Mech.* **39**, 1091 (1972).
8. J. M. Whitney and C. T. Sun, A refined theory for laminated anisotropic cylindrical shells. *J. Appl. Mech.* **41**, 471 (1974).
9. P. K. Sinha and A. K. Rath, Transverse bending of cross-ply laminated circular cylindrical plates. *J. Mech. Engng Sci.* **18**, 53 (1976).
10. J. N. Reddy, Exact solutions of moderately thick laminate shells. *J. Engng Mech. ASCE* **110**, 794 (1984).
11. P. Seide and P. H. H. Chang, Finite element analysis of laminated plates and shells. NASA-CR-157106, 157107 (1978).
12. S. T. Mau, P. Tong and T. H. H. Pian, Finite element solution for laminated thick plates. *J. Composite Mater.* **6**, 304 (1972).
13. R. L. Spilker, O. Orringer, E. A. Whitmer, S. Verbiese, S. E. French and A. Harris, Use of hybrid stress–finite element model for the static and dynamic analysis of multi-layer composite plates and shells, AMMRC CTR 76-29. ASRL TR 182-1, MIT, Cambridge, Massachusetts (1976).
14. R. A. Chaudhuri, An equilibrium method for prediction of transverse shear stresses in a thick laminated plate. *Comput. Struct.* **23**, 139 (1986).
15. P. Seide and R. A. Chaudhuri, Triangular finite element for analysis of thick laminated shells. *Int. J. Num. Meth. Engng*, to be published.
16. C. W. Pryor and R. M. Barker, A finite element analysis including transverse shear effects for application to laminated plates. *AIAA J.* **9**, 912 (1971).
17. R. A. Chaudhuri, Static analysis of fiber reinforced laminated plates and shells with shear deformation using quadratic triangular elements. Ph.D. Dissert., Department of Civil Engineering, USC, Los Angeles (1983).
18. Y. C. Fung, *Foundation of Solid Mechanics*. Prentice-Hall, Englewood Cliffs, New Jersey (1965).
19. J. T. Oden, *Finite Elements of Nonlinear Continua*. McGraw-Hill, New York (1971).
20. G. A. Korn and T. M. Korn, Differential geometry. In *Mathematical Handbook for Scientists and Engineers*, 2nd Edn, Chap. 17. McGraw-Hill, New York.
21. R. A. Chaudhuri and P. Seide, An approximate semi-analytical method for prediction of interlaminar shear stresses in an arbitrarily laminated thick plate. *Comput. Struct.* **25**, 627 (1987).
22. P. Seide, *Small Elastic Deformations of Thin Shells*. Noordhoff, Leyden, The Netherlands (1975).
23. R. A. Chaudhuri, K. Balaraman and V. X. Kunukkasseril, Arbitrarily laminated, anisotropic cylinder shell under internal pressure. *AIAA J.* **24**, 1851 (1986).

APPENDIX

This section presents some of the matrices and equations, referred to in the background information and theoretical formulation of this paper.

For anisotropic lamina with fiber orientation $\bar{\theta}_i$, the material or elastic stiffness matrix is given by[11, 17]

$$[C^{(i)}] = \begin{bmatrix} c_{11}^{(i)} & c_{12}^{(i)} & c_{13}^{(i)} & 0 & 0 \\ & c_{22}^{(i)} & c_{23}^{(i)} & 0 & 0 \\ & & c_{33}^{(i)} & 0 & 0 \\ & & & c_{44}^{(i)} & c_{43}^{(i)} \\ \text{Symm.} & & & & c_{55}^{(i)} \end{bmatrix}. \tag{A1}$$

The elements of $[C^{(l)}]$ can be obtained from the orthotropic material property matrix $[C^{(l)}]$ by a transformation of coordinates[11, 12]. The six non-vanishing elements can be expressed[12, 14] in terms of E_{11}, E_{22}, E_{12}, ν_{12}, G_{12}, G_{13} and G_{23}. Subscripts 1 and 2 denote directions parallel and perpendicular to the fiber, the 1–2 plane being tangential to a surface parallel to the reference surface of the shell, while subscript 3 denotes the direction normal to the reference surface.

$[A^{(l)}(\zeta)]$ referred to in eqn (1d) is given by[15, 17]

$$[A^{(l)}(\zeta)] = \begin{bmatrix} \frac{1-\zeta/t_l}{A_\alpha^{(l)}(\zeta)} & 0 & 0 & 0 & \frac{\zeta/t_l}{A_\alpha^{(l)}(\zeta)} & 0 & 0 & 0 & 0 & 0 \\ 0 & \frac{1-\zeta/t_l}{A_\beta^{(l)}(\zeta)} & 0 & 0 & 0 & \frac{\zeta/t_l}{A_\beta^{(l)}(\zeta)} & 0 & 0 & 0 & 0 \\ 0 & 0 & \frac{1-\zeta/t_l}{A_\alpha^{(l)}(\zeta)} & \frac{1-\zeta/t_l}{A_\beta^{(l)}(\zeta)} & 0 & 0 & \frac{\zeta/t_l}{A_\alpha^{(l)}(\zeta)} & \frac{\zeta/t_l}{A_\beta^{(l)}(\zeta)} & 0 & 0 \\ 0 & 0 & 0 & 0 & 0 & 0 & 0 & 0 & \frac{1}{A_\alpha^{(l)}(\zeta)} & 0 \\ 0 & 0 & 0 & 0 & 0 & 0 & 0 & 0 & 0 & \frac{1}{A_\beta^{(l)}(\zeta)} \end{bmatrix} \tag{A2}$$

where

$$A_\alpha^{(l)}(\zeta) = 1 + \frac{\bar{d}_l + \zeta}{R_\alpha} \tag{A3a}$$

$$A_\beta^{(l)}(\zeta) = 1 + \frac{\bar{d}_l + \zeta}{R_\beta}. \tag{A3b}$$

$\{\bar{\varepsilon}^{(l)}\}$ referred to in eqn (1d) can be written as[15, 17]

$$\{\bar{\varepsilon}^{(l)}\} = [B_j^{(l)}]\{d_j^{(l)}\}. \tag{A4a}$$

The matrix $[B_j^{(l)}]$ referred to in eqn (16) is

$$[B_j^i] = \begin{bmatrix} [R] & [O] & [Q] \\ [O] & [R] & [Q] \\ [M] & [N] & [T] \end{bmatrix} \tag{A4b}$$

where the submatrices [0] are (4×2) null matrices while the remaining submatrices are of the form

$$[x] = [[x_1] \ldots [x_k] \ldots [x_6]] \tag{A4c}$$

with

$$[R_k] = \begin{bmatrix} \frac{1}{g_\alpha}\Phi_{k,\alpha} & \frac{1}{g_\alpha g_\beta}\frac{\partial g_\alpha}{\alpha\beta}\Phi_k \\ \frac{1}{g_\alpha g_\beta}\frac{\partial g_\beta}{\partial\beta}\Phi_k & \frac{1}{g_\beta}\Phi_{k,\beta} \\ -\frac{1}{g_\alpha g_\beta}\frac{\partial g_\beta}{\partial\alpha}\Phi_k & \frac{1}{g_\alpha}\Phi_{k,\alpha} \\ \frac{1}{g_\beta}\Phi_{k,\beta} & -\frac{1}{g_\alpha g_\beta}\frac{\partial g_\alpha}{\partial\beta}\Phi_k \end{bmatrix} \tag{A5a}$$

$$[Q_k]^T = [\phi_k/R_\alpha \quad \phi_k/R_\beta \quad 0 \quad 0] \tag{A5b}$$

$$[T_k]^T = \begin{bmatrix} \frac{1}{g_\alpha}\phi_{k,\alpha} & \frac{1}{g_\beta}\phi_{k,\beta} \end{bmatrix} \tag{A5c}$$

$$[M_k^{(l)}] = \begin{bmatrix} -\frac{1}{t_l}\left(1 + \frac{\bar{d}_{l+1}}{R_\alpha}\right)\Phi_k & 0 \\ 0 & -\frac{1}{t_l}\left(1 + \frac{\bar{d}_{l+1}}{R_\beta}\right)\Phi_k \end{bmatrix} \tag{A5d}$$

$$[N_k^{(i)}] = \begin{bmatrix} \frac{1}{t_i}\left(1+\frac{\bar{d}_i}{R_\alpha}\right)\Phi_k & 0 \\ 0 & \frac{1}{t_i}\left(1+\frac{\bar{d}_i}{R_\alpha}\right)\Phi_k \end{bmatrix} \tag{A5e}$$

$i = 1, 2, \ldots, N, \quad k = 1, 2, \ldots, 6.$

The functions $f_1^{(i)}(\zeta)$ and $f_3^{(i)}(\zeta)$ referred to in eqn (21) are given by

$$f_1^{(i)}(\zeta) = -\frac{R_\alpha}{R_\Gamma R_{n\Gamma} t_i} F_1(\zeta) + \frac{(R_\alpha + \bar{d}_i + t_i)}{R_\Gamma R_{n\Gamma} t_i} R_\alpha F_2(\zeta) \tag{A6a}$$

$$f_3^{(i)}(\zeta) = -\frac{R_\alpha}{R_\Gamma R_{n\Gamma} t_i} F_3(\zeta) - \frac{(R_\alpha + \bar{d}_i + t_i)}{R_\Gamma R_{n\Gamma} t_i} F_2(\zeta) \tag{A6b}$$

where

$$F_1(\zeta) = \frac{(2a\zeta+b)}{4a}(a\zeta^2+b\zeta+c)^{1/2} + \frac{(4ac-b^2)}{8a^{3/2}} \ln |2\{a(a\zeta^2+b\zeta+c)\}^{1/2} + 2a\zeta + B| \tag{A7a}$$

$$F_2(\zeta) = (a\zeta^2+b\zeta+c)^{1/2} + \frac{(b-ad)}{2\sqrt{a}} \ln \left| \left\{ \frac{a\zeta+b}{\sqrt{a}} + (a\zeta^2+b\zeta+c)^{1/2} \right\} \right.$$
$$\left. - \frac{(c-bd+2ad^2)}{(ad^2-bd+c)^{1/2}} \ln \left| \frac{(b-2ad)\zeta + 2(c-bd)}{2(d+\zeta)} + \frac{(ad^2-bd+c)^{1/2}(a\zeta^2+b\zeta+c)^{1/2}}{(d+\zeta)} \right| \right. \tag{A7b}$$

with

$$a = R_{n\Gamma}^2 + R_\Gamma^2 \tag{A8a}$$

$$b = 2\{(R_\Gamma + \bar{d}_i) R_{n\Gamma}^2 + R_\Gamma^2 \bar{d}_i\} \tag{A8b}$$

$$c = \{R_{n\Gamma}^2 (R_\Gamma + \bar{d}_i)^2 + R_\Gamma^2 \bar{d}_i^2\}. \tag{A8c}$$